MAGNETIC FIELD EXPERIMENT FOR VOYAGERS 1 AND 2

K. W. BEHANNON, M. H. ACUNA, L. F. BURLAGA, R. P. LEPPING, and N. F. NESS

Laboratory for Extraterrestrial Physics, NASA-Goddard Space Flight Center, Greenbelt, Md 20771, *U.S.A.*

and

F. M. NEUBAUER

Institut für Geophysik und Meteorologie, Technische Universität, Braunschweig, F.R.G.

(Received 24 May, 1977)

Abstract. The magnetic field experiment to be carried on the Voyager 1 and 2 missions consists of dual low field (LFM) and high field magnetometer (HFM) systems. The dual systems provide greater reliability and, in the case of the LFM's, permit the separation of spacecraft magnetic fields from the ambient fields. Additional reliability is achieved through electronics redundancy. The wide dynamic ranges of ±0.5 G for the LFM's and ±20 G for the HFM's, low quantization uncertainty of ±0.002 γ ($\gamma = 10^{-5}$ G) in the most sensitive (±8 γ) LFM range, low sensor RMS noise level of 0.006 γ, and use of data compaction schemes to optimize the experiment information rate all combine to permit the study of a broad spectrum of phenomena during the mission. Objectives include the study of planetary fields at Jupiter, Saturn, and possibly Uranus; satellites of these planets; solar wind and satellite interactions with the planetary fields; and the large-scale structure and microscale characteristics of the interplanetary magnetic field. The interstellar field may also be measured.

1. Introduction

The investigations of the magnetic fields and magnetospheres of major planetary systems in the outer Solar System and their interactions with the solar wind are primary objectives of the space exploration program to be conducted during the Voyager missions. In addition, the investigation of interplanetary magnetic field phenomena during the flights is of fundamental importance both to the understanding of the magnetospheric observations and to a number of outstanding questions in basic plasma physics and in the general dynamics of the solar wind. If the Heliospheric boundary is penetrated, accurate measurement of the interstellar magnetic field is also an important objective.

A wide dynamic range, with high sensitivity for ultra-low field measurements, is required to accomplish both the planetary and interplanetary (and possibly also interstellar) objectives. The Voyager magnetic field experiment has been designed to provide precise, accurate and rapid vector measurements of fields ranging from 0.006 γ to 2×10^6 γ (20 G). To cover this enormous range efficiently, the experiment employs both a low field system and a high field system. The low field system has eight

Space Science Reviews **21** (1977) 235–257.

dynamic ranges from $\pm 8.8\ \gamma$ to $\pm 50\,000\ \gamma$ with corresponding quantization uncertainties of ± 2.2 mγ to $\pm 12.2\ \gamma$. The measured sensor noise level is 6 mγ RMS over a bandpass of 0–8.3 Hz. The basic instrument sampling rate is $16\frac{2}{3}$ vectors/sec. The high field system, whose sampling rate is $1\frac{2}{3}$ vectors/sec, has two dynamic ranges, ± 0.5 G and ± 20 G, with quantization uncertainties of $\pm 12.2\ \gamma$ and $\pm 488\ \gamma$, respectively, and a sensor noise level $< 10\ \gamma$ over a bandpass of 0–1 Hz.

Each 'system' consists of two complete magnetometer experiments; high reliability is obtained by the use of redundant subsystems and 'cross-strapping' between systems. The low field magnetometers are located remotely from the spacecraft on a 13 m boom, with sufficient separation to permit analytic removal of spacecraft fields from simultaneous measurements. This dual magnetometer technique, which was developed for and employed successfully on the Mariner 10 mission, has been described by Ness *et al.* (1971).

The major scientific objectives of the Voyager magnetic field experiment may be summarized as follows:

(1) Measure and analytically represent the planetary magnetic fields of Jupiter, Saturn, and possibly Uranus. Use these observations to continue and extend comparative studies of planetary magnetism.

(2) Determine the magnetospheric structure of all planets encountered. Investigate the basic physical mechanisms and processes involved, both in solar wind-magnetosphere interactions and internal magnetospheric dynamics, in correlative studies with other particles and fields experiments.

(3) Investigate the interactions of the satellites of these planets with their magnetosphere/solar wind environments. Assess the role of such interactions in observed magnetospheric phenomena and deduce physical properties of the satellites encountered, especially possible intrinsic magnetization.

(4) Accurately survey the interplanetary magnetic field beyond 1 AU and continue and extend studies of the large-scale characteristics of the interplanetary medium. In particular, the evolution and detailed properties of solar wind streams and their effects on planetary magnetospheres will be investigated.

(5) Continue and extend studies of the physics of microscale phenomena in the solar wind. In particular, studies of the properties of waves, shocks, and directional discontinuities will be conducted and the relation between the magnetic field and the propagation of solar and galactic cosmic rays investigated.

(6) Search for the transition between the interplanetary and interstellar media, and, if possible, investigate the characteristics of the boundary region and measure the galactic magnetic field and its variations.

All of the results will be considered in terms of their significance for theories of the origin of the Solar System and for their general applicability to other areas of astrophysics.

The specific objectives are discussed in more detail in Sections 2 through 4, and the experiment instrumentation and data characteristics are described in detail in Section 5.

2. Jupiter Science Objectives

2.1. Magnetosphere

One of the most remarkable results of the Pioneer 10 and 11 flyby missions was the identification of a strongly distorted outer magnetosphere of the planet Jupiter (Smith *et al.*, 1974, 1975, 1976a). Nevertheless, the three-dimensional characteristics of the Jovian magnetosphere are still by no means well understood. The post-Pioneer picture of magnetospheric structure is in contrast with pre-encounter expectations and has raised profound questions about the physics of Jupiter's magnetosphere, particularly with regard to the influence of the rapid rotation of the massive planet.

The Voyager missions will provide another pair of traverses through the interesting and important outer magnetospheric region. In this case, a unique separation of the spatial and temporal variations may be possible because of the relatively close spacing of the two Voyager spacecraft, allowing the state of the near-Jupiter interplanetary medium to be monitored by one spacecraft during the magnetospheric traverse of the other. Since the inclination of Jupiter's rotational axis to the ecliptic is only 3° and the tilt of its dipole axis approximately 9.5°, the wobbling of the solar wind flow direction relative to a magnetospheric frame of reference is less than that at Earth. Hence, any significant variation of the magnetospheric structure observed by the Voyagers, in comparison with earlier investigations, can be most plausibly interpreted in terms of different conditions of the magnetosphere and interplanetary medium at that time rather than any significant difference in flow geometry relative to the magnetic field source.

From the Pioneer observations, the Jovian magnetosphere has been interpreted as being a very 'soft', although an enormously large, obstacle to solar wind flow. This view is based on the wide variation in the radial distances of the observed multiple bow shock and magnetopause crossings (Smith *et al.*, 1974, 1975; Wolfe *et al.*, 1974). This is illustrated in Figure 1 by the Pioneer 11 magnetic field measurements (Smith *et al.*, 1975). Such large excursions of the bow shock and magnetopause positions might be a general feature of the Jovian magnetosphere and may be produced by the interaction with the steep stream interfaces or shock pairs that are associated with high-speed solar wind streams at large heliocentric distances (Hundhausen and Gosling, 1976). Internal dynamical processes may also be involved in the magnetopause position changes. Correlative observations by the two Voyager spacecraft should provide additional insight into the characteristics of these phenomena.

The highly fluctuating fields associated with the microscale physical processes of the solar wind-outer magnetosphere interaction will be studied in detail. Such detailed structure is illustrated in Figure 2, which shows Pioneer 10 total magnetic field measurements during a three-day period which included a single set of bow shock and magnetopause crossings. The data will be investigated for evidence of plasma instabilities in the magnetopause region. The detailed study will include an

analysis of any bow shock-associated waves similar to those observed at Earth (see reviews by Fairfield, 1976; Greenstadt, 1976) and near Mercury (Fairfield and Behannon, 1976), as well as any waves that may be observed within the outer magnetosphere.

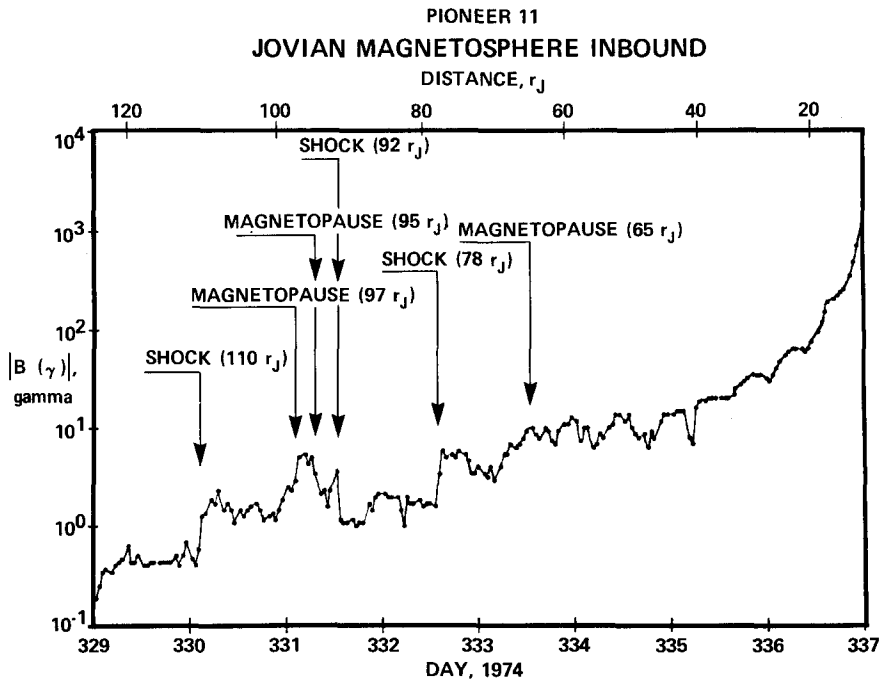

Fig. 1. Pioneer 11 one-hour averages of magnetic field magnitude (Smith *et al.*, 1975) inbound at Jupiter, illustrating multiple bow shock and magnetopause crossings over a period of five days and a distance range of $32R_J$.

Voyager 1 and 2 will provide additional observations of the structure of the Jovian magnetosphere to a closest approach radius of $4.9R_J$. Beyond $10–12R_J$, the planetary field was found by Pioneers 10 and 11 to be increasingly distorted from a dipole configuration with increasing distance from the planet. It appears to be extended or distended by a disc-like plasma distribution which has been discussed theoretically by Barish and Smith (1975), Goertz (1976), and Gleeson and Axford (1976). This configuration is similar to the geomagnetic tail, and beyond approximately $30R_J$ a thin (perhaps $1–2R_J$ thick), low magnitude ($\sim 1\gamma$) current sheet region exists. The existence of a tail-like configuration in the region so far explored (5–12 hr local time) is thought to result from the large centrifugal force associated with the vast magnetosphere and rapid (10 hour) planetary rotation rate. This force causes the magnetic field lines to extend far out near the equatorial plane. At large distances from Jupiter outward plasma flow along the field lines may be a possible explanation for the observed spiral field structure. Radiation belt particle observations during the Pioneer mission suggest the corotation region to extend out to approximately $25R_J$

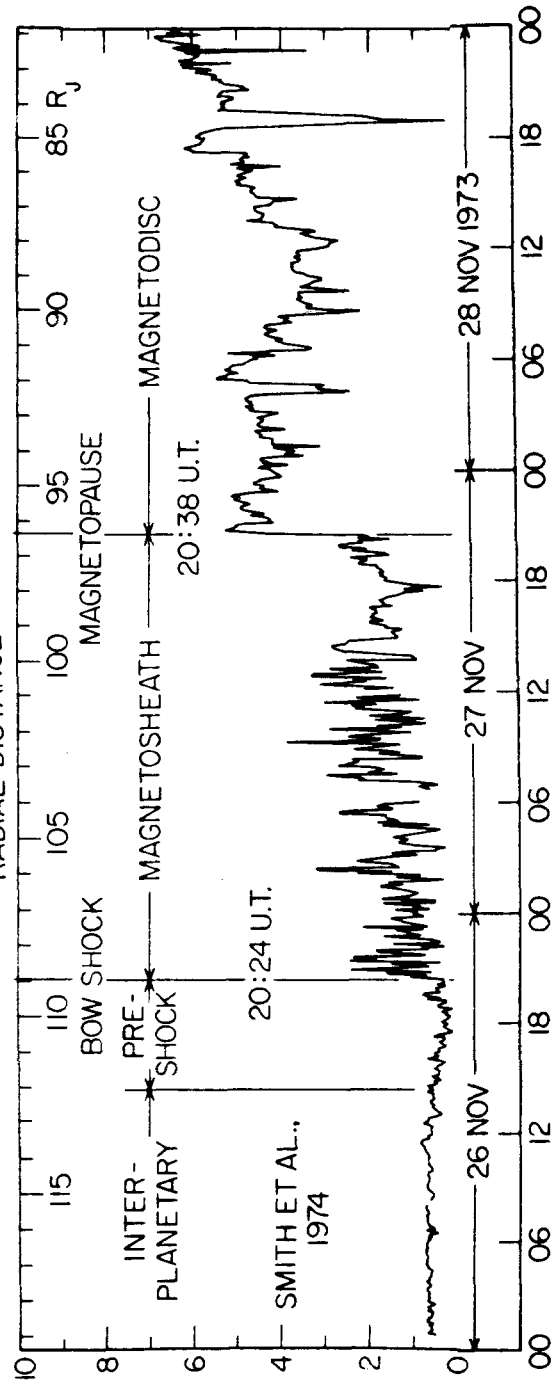

Fig. 2. Detailed measurements of magnetic field magnitude by Pioneer 10 inbound, showing the complex field structure in the region of interaction between the solar wind and the outer Jovian magnetosphere. A distinct pre-shock region of fluctuating fields was observed, followed by a stronger but highly variable field in the sheath region. A 'turbulent' region just inside the magnetopause was found to be an additional feature of this complex interaction. Investigation of the physics of such regions are among the objectives for Voyager spacecraft encounters with Jupiter. Similar detailed interaction studies will be conducted at Saturn and possibly Uranus.

(e.g. Trainor *et al.*, 1974). The Voyager observations will provide further information on this point. A better understanding of the extent of 'wrapping up' or 'spiraling' of the magnetic field in the outer Jovian magnetosphere will permit determination of the angular momentum transfer between the solar wind and Jupiter.

2.2. Satellite-magnetosphere interactions

The interaction between a satellite and the Jovian magnetosphere depends on the properties of the satellite and its atmosphere, on the characteristics of the field and particle environment, and on the properties of the Jovian ionosphere. Since the Jovian magnetosphere probably co-rotates with the planet at least to the orbit of Callisto (e.g., Trainor *et al.*, 1974), the relative velocities between satellites and plasma are 57, 104, 199, and 333 km sec^{-1} for Io through Callisto, respectively. Bow shocks will form in this interaction if $V_{rel} > \sqrt{(V_A^2 + V_s^2)}$ (V_A and V_s are the Alfvén and sound speeds, respectively), since the relative velocity is roughly perpendicular to the local magnetic field. Unless the tentative density measurements from Pioneer (Frank *et al.*, 1976) are wrong by more than two orders of magnitude, $V_{rel} \ll \sqrt{(V_A^2 + V_s^2)}$ and therefore the speeds of the inner three Galilean satellites are sub-fast in the MHD sense. It is only for Callisto that a slight increase in the plasma density and decrease in proton temperature below the measured value of $kT_p =$ 400 eV in the plasma sheet would allow $V_{rel} \gtrsim \sqrt{(V_A^2 + V_s^2)}$. Hence we expect no bow shock at Io, Europa, and Ganymede but possibly at Callisto as it moves through the equatorial plasma sheet.

The origin of the decametric emissions from Jupiter remains an outstanding problem. These bursts, with a peak near 8 MHz and reaching into the hectometric region, are probably connected with plasma instabilities within the Jovian ionosphere (Smith, 1976). The control of the decametric emissions by Io is most likely exercised by means of the magnetic flux tube connecting a plasma sheath around Io with Jupiter's ionosphere. The foot of this tube probably produces or enhances instabilities in the ionosphere and hence influences the production of decametric bursts. Various unipolar induction models of the interaction have been developed by Goldreich and Lynden-Bell (1969), Gurnett (1972), Webster *et al.* (1972), Neubauer and Luzemann (1977) and Shawhan (1976).

The Voyager 2 spacecraft is targeted to traverse the Io fluxtube at a distance of 25 000 km from Io and thus should provide a definitive observation of phenomena related to decametric radiation. A diagram of this traverse, in which a maximum of 4 min 30 sec will be spent in the fluxtube, is included in the Mission Description. The sketch shows that the position predicted for the fluxtube depends on the Jupiter main field model used, i.e., whether it is that of Smith *et al.* (1976a) or that of Acuna and Ness (1976b). For the case shown in the figure, where only the equivalent offset tilted dipole was used, the difference in predicted position is mainly a shift along the trajectory path, and hence the probability of intercepting the fluxtube is model independent. We note in addition that the field-aligned currents predicted by most models of the Io-magnetosphere interaction cause a bending of the fluxtube which is

particularly strong near Io. The fluxtube leaves Io tilted away from the undistorted magnetic field by the angle δ in the direction of the orbital motion of Io. A rough estimate of the bending due to field-aligned currents to and from Jupiter leads to an angle $\delta \approx 3° \times$ current in million amperes. Careful analysis of the flyby magnetic field data will enable us to develop a model description of the current system in the vicinity of Io. For example, a current of 800 000 amperes will lead to a displacement of the fluxtube cross-section by 30% of one Io diameter at about 25 000 km from the satellite.

In physical models of the Io–Jovian magnetosphere interaction, the assumption has tacitly been made that Io has no internal magnetic field. There is no observational evidence either for or against such an assumption. However, the rocky satellites Io and Europa should at least contain certain amounts of magnetizable material. Thus Io could possibly possess either fields due to a natural remanent magnetization, a dynamo field, or an induced field. In the interpretation of the Io flyby data, various models of an internal magnetic field will be considered.

Another relatively near satellite encounter will be the flyby of Ganymede, with a targeted closest approach radius of 50 000 km for Voyager 1. Ganymede is considered second in interest among the Galilean satellites because of the recent evidence for an atmosphere which may be composed of oxygen (Yung and McElroy, 1975). Measurements taken near Ganymede will be studied for evidence of interaction-related disturbances. As at Io, we shall also look for evidence of an internal magnetic field.

2.3. Main magnetic field

Jupiter was studied by radio astronomical means for almost two decades before the first direct information on Jupiter's magnetic field was provided by the Pioneer 10 and 11 flybys in 1973 and 1974. These spacecraft confirmed many characteristic features of the magnetic field of Jupiter (Smith *et al.*, 1974, 1975, 1976a; Acuna and Ness, 1976a,b) and established the dipole moment as $\approx 1.6 \times 10^{30}$ G cm^{-3}, tilted $\sim 9.5°$ near the appropriate system III longitude, taking into account the slight difference between the rotation rate of the magnetic pole relative to the system III rotation rate (Mead, 1974).

Analyses of magnetic field data obtained close to the planet (i.e., at distances of less than $6R_J$) have been conducted in terms of a classical spherical harmonic expansion of magnetic multipoles. Results from the two separate Pioneer 11 experiments of Acuna and Ness (1976a,b) and Smith *et al.* (1976a) agree with respect to the significance of the surprisingly large quadrupole and octupole terms. The closest approach during the Voyager flybys will be at a distance of $4.9R_J$, and at that distance the main magnetic field is dominated by the dipole term, with small contributions from magnetic field sources external to the planet. The latter include the distortion of the Jovian magnetosphere by planetary rotation, plasma co-rotation and inflation, and the interaction with the solar wind. It is possible that a careful comparison of accurate analyses of data from Pioneers 10 and 11 and Voyagers 1 and

2 will provide a data base for studying any secular change of the Jovian magnetic field.

3. Saturn Science Objectives/Uranus Option

3.1. Main field and magnetosphere of Saturn

Since Saturn is similar to Jupiter in terms of size, rotation period, low mean density and probable internal heat source, it is reasonable to infer that Saturn may also have an intrinsic magnetic field and magnetosphere similar to that of Jupiter. Assuming that the magnetic dipole moment of a planet is proportional to its angular momentum, simply scaling from Jupiter results in the prediction of a dipole moment of approximately 1×10^{30} G cm$^{-3} = 4$ G R_S^3, with 9 G polar surface field.

The first unambiguous evidence for a Saturnian magnetic field has been found by the IMP-6 observation of non-thermal radio emission near 1 MHz (Brown, 1975). The peak flux density near 1 MHz is nearly equal to that found for Jupiter at 8 MHz when the difference in distance from the Earth is taken into account. The frequency difference is most likely related to a difference in planetary magnetic field strengths. If linear scaling is appropriate, as would be the case for cyclotron emission, Saturn's magnetic field would be lower than Jupiter's by a factor of 8, giving a Saturnian polar field in the range 1–2 G. The dipole moment would scale as $M_S = \frac{1}{8}(R_S/R_J)^3 M_J$, yielding $M_S = 1 \times 10^{29}$ G cm$^{-3} = 0.5$ G R_S^3.

The major objective of the magnetic field experiment during the encounters of the two Voyager spacecraft with Saturn will be the measurement of the intrinsic Saturnian magnetic field. As in the case of Jupiter, the Saturnian field will be investigated by determining the leading coefficients of the spherical harmonic expansion for the magnetic field. A closest approach distance of $3.3R_S$ is targeted for Saturn (or $2.7R_S$ if the Uranus option is exercised). An analysis of the encounter trajectories for various field models has shown that the latitude and longitude coverages are great enough for those trajectories to permit the determination of a quadrupole component and probably also an octupole component of the planetary field (Thompson and Ness, 1977).

Many of the objectives for the study of the magnetosphere of Jupiter are also applicable to Saturn. Although no magnetospheric models exist for Saturn, with a dipole moment $M_S = 1 \times 10^{29}$ G cm^3 perpendicular to the solar wind and for expected typical solar wind properties at 10 AU, we would expect the stagnation point to be located at a distance of $\sim 25R_S$ with a field magnitude of 7 γ just inside the magnetopause for a magnetosphere of the terrestrial type. For comparison, a stagnation point distance of $\sim 50R_S$ is obtained using the dipole moment derived from angular momentum scaling. The effects of the rapid planetary rotation (10-hour period) will be investigated. A much larger magnetosphere is expected if stretching of field lines due to centrifugal forces is important. Details of such a magnetosphere depend on a detailed model for the plasma distribution in the magnetosphere of Saturn.

3.2. Satellite studies

In the same manner as at Jupiter, the effects of satellites on the magnetosphere will be investigated. In the case of Saturn the major difference is the absence of a big satellite like Io close to the planet. Titan is the major satellite targeted for investigation, and the semimajor axis of its orbit about Saturn is $20R_S$. If the Saturnian magnetic field is in fact as strong as is implied by the non-thermal emission data, then Titan will probably be inside the magnetosphere of Saturn at least during periods of undisturbed solar wind conditions. Titan is somewhat larger and more massive than the Moon, and it has been long known to have a gravitationally-bound atmosphere. Thus the interaction of Titan with its environment will be of special significance.

Both spacecraft will encounter Titan prior to Saturn closest approach, in the sunward part of the Saturnian magnetosphere, with a Titan closest-approach distance of 7000 km $\simeq 3R_T$. The trajectories will traverse both the expected nominal position of a 'wake' produced by corotation of the Saturnian magnetosphere and the solar occultation shadow region (see the Titan encounter diagram in the Mission Description). The former will provide the most significant magnetic field measurements for investigation of the interaction of Titan with Saturn's magnetosphere. In the event that Saturn has a significantly weaker magnetic field than is now expected, or if the magnetopause is temporarily closer to the planet in response to an increased solar wind ram pressure, the latter traversal will permit measurements of Titan's wake in the solar wind. The nature of the wake observed in either case should make it possible to infer at least an upper limit for an intrinsic magnetic field of Titan. It may also be possible to detect a bow shock wave upstream of Titan if one exists.

It is doubtful whether any significant magnetic effects will be observed during any of the other Saturnian satellite flybys due to the small sizes of the satellites, the greater encounter distances and generally less favorable encounter phases.

3.3. Uranus objectives

The option to reprogram Voyager 1 inflight for a Uranus encounter has been discussed in the Mission Description. This possibility is of particular interest to magnetic field investigators because of the recent indication that Uranus also may have a strong magnetic field. Brown (1976) has reported the detection by IMP-6 of radio bursts from the direction of Uranus. These emissions are similar to those originating from Jupiter and Saturn, but the observations are ambiguous because of the unfavorable angular separation of Earth and Uranus during the observing period. The uniqueness of the events suggests that the source is not terrestrial, however. The observed events were strongest in intensity near 0.5 MHz. The spectral behavior was similar to that of emissions from Jupiter and Saturn except for a smaller bandwidth. With linear scaling, the polar field for Uranus would be less

than that inferred for Saturn by a factor of 2 and thus 16 times lower in magnitude than that of Jupiter. The magnetic moment would scale as $M_U = \frac{1}{16}(R_U/R_J)^3 M_J$, yielding $M_U = 3 \times 10^{27}$ G cm^{-3} or 0.2 G R_U^3.

The main objective at Uranus would be the determination of the planetary magnetic field. Uranus is distinctive among the planets in that its axis of rotation lies very nearly in the ecliptic plane. This orientation of the rotation axis together with the rapid rotation (~11 hour period) and the spacecraft flyby speed and path will yield excellent longitude and latitude coverage. This is very favorable for the determination of a reasonable set of low order spherical harmonic coefficients to describe the internal magnetic field.

Prior to the existence of any observational evidence for a magnetic field at Uranus, models of a possible Uranian magnetosphere were constructed by Siscoe (1975) as a function of dipole moment M_U for $2 \times 10^{-3} M_E \leq M_U \leq M_J$, where M_E = Earth's magnetic moment. If the magnetic moment inferred from the observations of Brown (1976) is correct, the models predict that the magnetosphere encloses the orbit of the outermost satellite, Oberon.

Although there are uncertainties in boundary conditions and thus a large number of possibilities for any Uranian magnetosphere, the unique orientation of the Uranian rotation axis makes such a magnetosphere extremely interesting in comparison with other magnetospheres. It is likely that its magnetic dipole axis is aligned close to its rotation axis as is the case for Earth and Jupiter. In the present 84 year orbit of Uranus about the Sun, the rotational axis and therefore probably also approximately the dipole axis will be aligned roughly along the Uranus–Sun line in 1985. Thus the dipole axis should be within 10° of this unique alignment at the time of flyby by the Voyager 1 spacecraft flying the Uranus option, offering the opportunity to probe a 'pole-on' magnetosphere when the pole is close to Sunward orientation.

For such a configuration the magnetosphere should be characterized by steady magnetospheric convection because the geometric conditions for reconnection taking place at the magnetopause are essentially always fulfilled. Since reconnection is one of the important basic processes in space plasma physics, the study of this magnetosphere would be an important objective of the magnetic field experiment at Uranus. Inside the magnetosphere, the rapid rotation of the planet combined with the solar wind-induced convection will lead to strongly distorted field lines. The solar wind conditions determining the convection picture will have been observed shortly before encounter.

The low interplanetary fields expected at Uranus mean that the electron gyrofrequency in the region just upstream from the planet (2.8 Hz in a 0.1 γ field) will fall well within the bandpass (Nyquist frequency) of the instrument in the encounter mode. In the event of a planetary bow shock, not only can the types of lower-frequency upstream wave associated with other planetary bow shocks be studied but other types of waves nearer the electron gyrofrequency also can be investigated.

4. Interplanetary Magnetic Field Observations

The Voyager missions provide an opportunity to study magnetic fields in a 'collisionless' plasma on a wide astronomical scale (to a distance of at least 10 AU and possibly to 20 AU and beyond). In contrast with the approximately one year launch separation of Pioneers 10 and 11, the two Voyager flights will be launched less than one month apart. This will provide a unique opportunity to study the general evolution, including propagation and dissipation characteristics, of waves, discontinuities, shocks and large-scale stream-related features of the interplanetary magnetic field in a way unmatched by previous missions.

Perhaps the most interesting large-scale feature that might be observed is the transition between the interplanetary magnetic field and the interstellar magnetic field. The best current estimate is that this occurs by means of a shock at 50 AU (Axford, 1973), which is well beyond the limits of the Voyager missions, but the estimate of 50 AU could be in error by a factor of 2. Hence the possibility exists that the Voyager spacecraft will traverse the transition region and even measure the galactic magnetic field and its variations. Since the average galactic field in the region sampled might be less than 0.1 γ (Vershuur, 1968; Bok, 1970), it is important to be able to measure fields of this strength and weaker.

Large time variations in the solar wind and interplanetary field parameters are continuous features of the interplanetary medium and are of primary importance to the dynamical behavior of planetary magnetospheres as well as to interplanetary dynamical processes. The principle variations in energy density of the magnetic field near 1 AU are related to 'corotating' streams of high speed solar plasma. Such streams often steepen to form shock pairs beyond 1 AU (Smith and Wolfe, 1976; Hundhausen and Gosling, 1976; Gosling *et al.*, 1976).

Flare-associated streams preceded by a shock (Hundhausen, 1972; Burlaga, 1975) or a shock pair (Ipavich and Lepping, 1975) are observed near 1 AU and have been observed beyond 1 AU by Pioneer 10 (Smith *et al.*, 1976b). An important complication in the distant solar wind is the interaction of flare-associated streams with corotating streams. The study of both types of streams and shocks as they occur, and their evolution through successive interactions, will be facilitated by the dual-spacecraft observational capability of the Voyager missions.

The microscale properties of the magnetic field are of fundamental importance to a number of basic processes in the solar wind such as heat transport, wave propagation and the motion of energetic solar particles and galactic cosmic rays throughout the solar system. The Voyager magnetic field experiment is designed to permit detailed studies of microstructure in the distant interplanetary and even intergalactic fields (see Section 5), and such studies will be carried out in close collaboration with plasma and energetic particles investigators. Among the phenomena to be investigated are the origin, growth, motion and dissipation of MHD and plasma waves, magnetic field annihilation and reconnection, discontinuities, interactions between magnetic fields and energetic particles, effects of the field on the proton and electron distribution

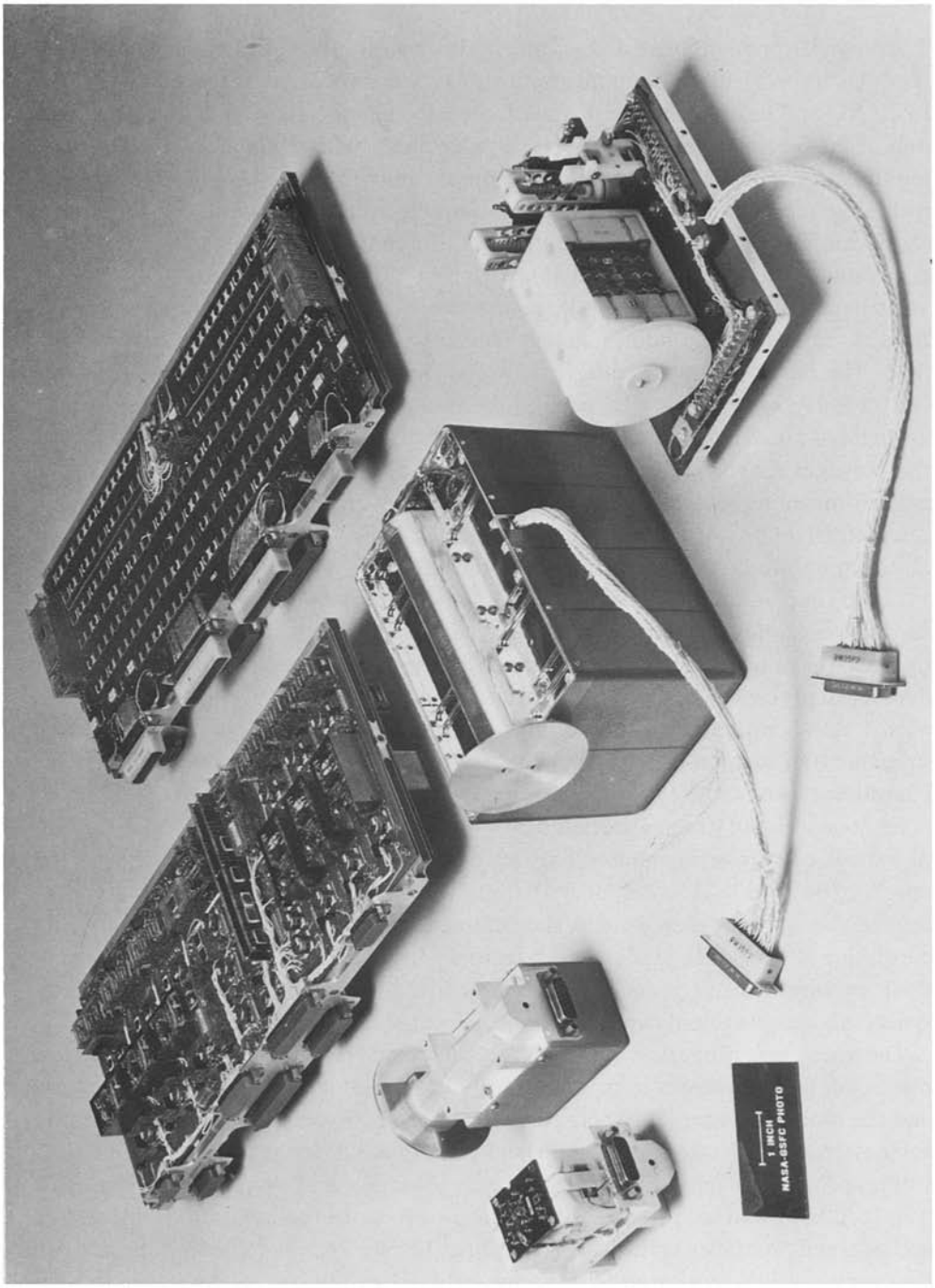
1 INCH
NASA-GSFC PHOTO

functions of the plasma, and the general properties of a 'collisionless', neutral hydrogen-plasma mixture and a magnetic field.

5. Instrument Description

5.1. General configuration

The NASA-GSFC magnetic field experiment on Voyagers 1 and 2 consists of two magnetometer systems: the high field magnetometer (HFM) and the low field magnetometer (LFM). Each system contains two identical triaxial fluxgate magnetometers which measure the magnetic field intensity along three mutually orthogonal axes simultaneously. The instruments represent the latest stage in the continuous program of magnetometer development within our laboratory. The choice of fluxgate magnetometers is based upon more than 13 years of highly satisfactory experience with such detectors within this group. They provide accurate direct vector measurements of ambient magnetic fields while requiring minimum electronic circuitry, weight and power.

Both high and low field magnetometer sensors utilize a ring core geometry and thus have lower drive power requirements and better zero level stability than other types of fluxgates and are smaller in size (Acuna, 1974). The cores consist of an advanced molybdenum alloy, especially developed in cooperation with the Naval Surface Weapons Center, White Oak, Maryland, which exhibits extremely low noise and high stability characteristics. The use of this alloy and the ring core sensor geometry thus allows the realization of compact, low power, ultrastable fluxgate sensors with a noise performance that is improved almost an order of magnitude over the best previously flown fluxgate sensors. The HFM's use specially processed miniature ring cores (1 cm diameter) which minimize the power required to measure large fields.

One LFM is located at the outboard end of the magnetometer boom and the other is mounted inboard at approximately 0.57 the distance from the boom-spacecraft interface to the outboard LFM. The total interface-to-tip boom length is 13 meters. The two HFM's are located approximately one meter apart along the boom support truss. The remote location of the LFM's reduces magnetic contamination from the spacecraft. The experiment is shown in Figure 3. The total weight, sensors plus electronics, is 5.6 kg and the power required is 2.2 W.

5.2. Dual magnetometer concept

The dual magnetometer configuration, developed by Ness *et al.* (1971) for the Mariner 10 mission and conceptually generalized by Neubauer (1975), permits

Fig. 3 (opposite). Flight hardware for one Voyager spacecraft. At the top are the bus-mounted analog (left) and digital (right) electronics subchassis. At the lower left are shown the two High Field Magnetometers, with the two Low Field Magnetometers at the lower right. One of each type of magnetometer is shown enclosed in its flight canister with attached RHU (radioactive heating unit) housing. Note the mechanical flipper assembly on the LFM at the right.

analytic separation of the spacecraft field from the ambient field. In application of the dual magnetometer concept, it is assumed that, to a good approximation, the magnetic field of the spacecraft is a spacecraft-centered dipole field as measured at the remote location of the magnetometer sensors. The spacecraft field at the position of the outer magnetometer is estimated using

$$\mathbf{B}_{sc}^{est}(r_2) = \alpha \frac{[\mathbf{B}_{obs}(r_1) - \mathbf{B}_{obs}(r_2)]}{1-\alpha}$$

where $\mathbf{B}_{obs}(r_i)$ is the measured field at r_i, $i = 1$ or 2 representing inner or outer position respectively, and where the coupling coefficient α is in this case given by $\alpha = (r_1/r_2)^3$. This analytically determined vector spacecraft field at r_2 is then subtracted from the outboard magnetometer measurements, yielding an estimate of the ambient magnetic field. This method thus permits the removal from the measurements of the effects of a significant and variable spacecraft field on a continuous basis throughout the mission. The spacecraft field at r_2 is expected to be approximately 0.2 γ.

5.3. Sensor alignment calibration

The 13-meter magnetometer Astromast booms have proved in extensive pre-flight testing to be highly rigid with respect to bending motions but 'soft' to torsional or twisting motion. Deployment repeatability tests have shown as much as $\pm 7°$ uncertainty in knowledge of the boom 'twist' angle (about the boom axis) at the magnetometer sensor positions, compared with approximately $\pm 0.5°$ uncertainty in bend angles (rotation about axes orthogonal to the boom axis). In order to minimize sensor alignment uncertainties, a method to estimate an angular correction matrix was developed that eliminates most of the twist uncertainty and some of the bend uncertainty.

A special calibration coil has been wound around the periphery of the spacecraft's high gain antenna to generate, upon command, a known magnetic field at both LFM magnetometer sensors. The difference between measurements taken when the coil is turned on and off is the coil field, independent of all external fields. Using a 20 turn coil of $\frac{1}{2}$ amp yields nominal field intensities of 33.4 and 6.1 γ at the inboard and outboard sensors, respectively.

An angular correction matrix cannot be uniquely determined from data obtained through the use of a *single* reference coil. Thus, the method that has been developed estimates an angular correction matrix which *optimally* corrects for misalignment. This is possible because (1) in the rotation corrections the small-angle approximation is permitted, eliminating the usual problem of incommutability of rotations, and (2) the twist angle is known to strongly dominate the uncertainty. With such a scheme the angular correction matrix takes the following form:

$$\mathbf{M} = \begin{pmatrix} 1 & -\varepsilon & 0 \\ \varepsilon & 1 & -\delta \\ 0 & \delta & 1 \end{pmatrix}$$

where

$$\varepsilon \approx 2\left(\frac{\Delta B_X^M - \Delta B_X^T}{\Delta B_Y^M + \Delta B_Y^T}\right) \quad \text{is the twist angle, and}$$

$$\delta \approx 2\left(\frac{\Delta B_Z^M - \Delta B_Z^T}{\Delta B_Y^M + \Delta B_Y^T}\right) \quad \text{is one of the bend angles.}$$

The superscripts M and T represent inflight measured and theoretically determined coil fields, $\hat{Z}$ is aligned with the boom axis, $\hat{X}$ and $\hat{Y}$ are orthogonal to $\hat{Z}$ and to each other but otherwise arbitrary; the second bend angle is set equal to zero. Simulation studies have shown that application of this additional calibration procedure reduces the twist uncertainty to $\pm 0.25°$ (including quantization uncertainty of the instrument) and the bend uncertainty to less than $\pm 0.5°$.

5.4. Redundant electronics

The experiment electronics instrumentation consists of the flux-gate magnetometer electronics and associated controls, and the calibration and data processing electronics. The electronics block diagram is shown in Figure 4. Complete redundancy is provided for the analog to digital converters, data and status readout buffers, command decoders and power converters. Thus not only can the two magnetometers of a system be interchanged, but considerable cross-strapping within the electronics permits interchange of critical internal functions as well. This design significantly reduces the impact of single-component failure on the ability of the experiment to continue successful operation during the mission duration of $\geqslant 4$ years.

5.5. Measurement range and accuracy

To meet the scientific objectives of the investigation, a wide total dynamic range of ± 20 G was selected, together with 12-bit digital resolution. The LFM's cover the range ± 0.5 G and the HFM's extend the experiment range to ± 20 G. To optimize sensitivity at low field values, the total LFM range was divided into eight dynamic ranges and the total HFM range into two dynamic ranges. The individual ranges and associated quantization uncertainties are given in Table I. These dynamic ranges will be switched automatically whenever the combined ambient field plus fluctuations exceeds a predetermined level. The automatic range switching strategy is shown schematically in Figure 5. Automatic range switching can be overridden by ground command.

The extremely low digitization uncertainty in the lowest LFM range will permit the precise and accurate measurement of the very weak fields expected in the distant solar wind and also the interstellar fields beyond the heliospheric boundary. The achievement of these goals will be limited only by zero offset uncertainty and the intrinsic noise levels of the sensors themselves and the accuracy of the spacecraft field correction procedures. The Voyager sensor zero offset variations have been found to be less than $\pm 0.2\ \gamma$ over the temperature range of -60 °C to $+60$ °C.

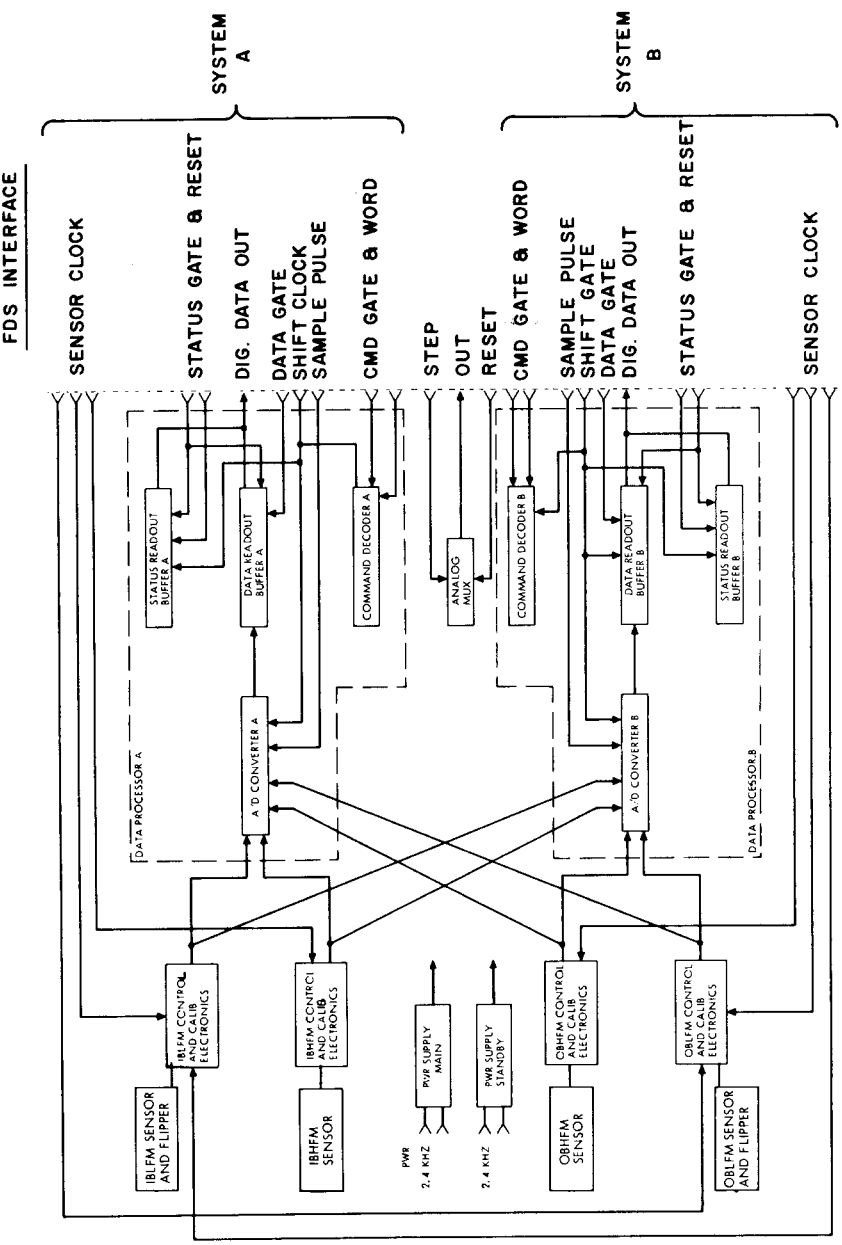

Fig. 4. Block diagram of the magnetic field experiment. System A consists of the inboard (IB) LFM and HFM systems and system B includes the outboard (OB) LFM and HFM systems, along with their respective data processors. The cross-strapping that exists between magnetometers and data processors is shown.

TABLE I

Range	Quantization
LFM Dynamic ranges and quantization uncertainty:	
1. ±8.8 γ	±2.2 mγ
2. ±26 γ	±6.3 mγ
3. ±79 γ	±19 mγ
4. ±240 γ	±59 mγ
5. ±710 γ	±173 mγ
6. ±2100 γ	±513 mγ
7. ±6400 γ	±1.56 γ
8. ±50,000 γ	±12.2 γ
HFM Dynamic ranges and quantization uncertainty:	
1. ±0.5 G	±12.3 γ
2. ±20 G	±488 γ

The incorporation of both mechanical and electrical 'flippers' into the experiment will permit the correction for any offsets that might occur during the mission to an accuracy of ±0.05 γ. Each LFM is equipped with an electrothermally-controlled spring mechanism to rotate the sensors for inflight *sensor* offset determination. In addition, each LFM is equipped with an electrical flipper to reverse sensor signal

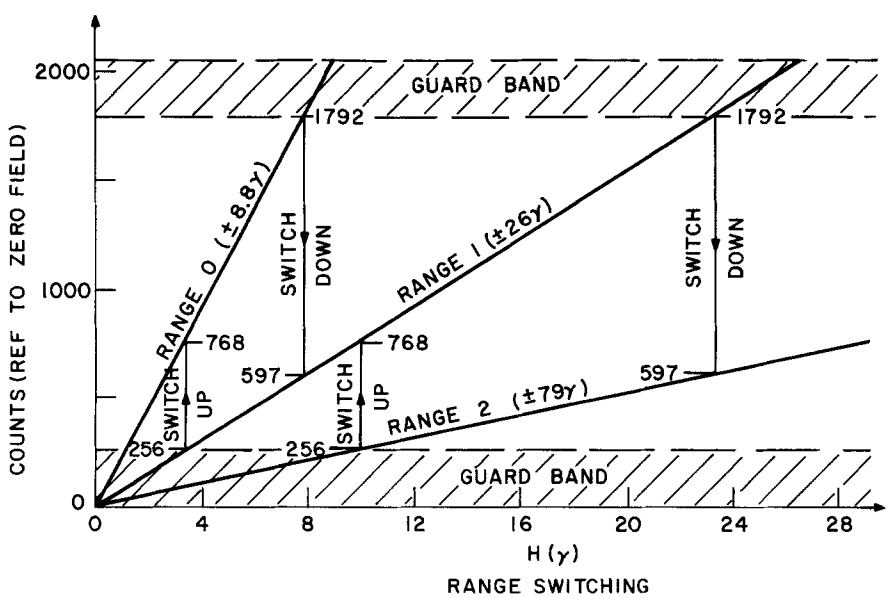

Fig. 5. Illustration of a portion of the total magnetometer automatic range switching strategy. For operation within a given range, when the detected field strength exceeds the lower bound of the upper guardband (1792 engineering units or counts), automatic switching down to the next less sensitive range occurs. Similarly, a measurement that is lower than the upper bound on the lower guardband (256 counts) automatically initiates a switch up to the next more sensitive range.

polarity for inflight *electrical* zero offset determination. In the latter case, the offsets detected would be those due to radiation effects, component aging, and temperature and voltage variations, but not those due to changes in the magnetic properties of the materials used in the sensors. During extensive sensor testing, zero drifts due to changes in magnetic properties have been found to be less than 0.1 γ over a $\frac{1}{2}$ year period. The sensitivity of each magnetometer is checked periodically by the generation of precisely calibrated fields by coils carrying accurately known currents.

A typical sensor noise level is 0.006 γ RMS over a 8.3 Hz bandwidth; this performance is illustrated in Figure 6. Figure 6(a) shows the response of the instrument to inputs of 1, 0.5, 0.25, 0.125, and 0.062 γ, while Figure 6(b) shows the

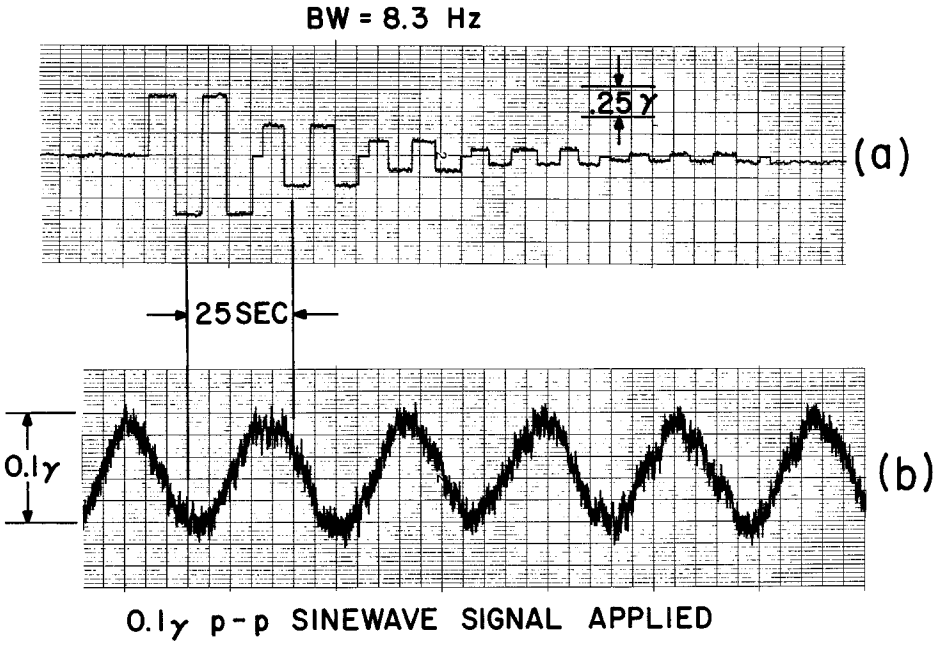

NOISE	BW = 8.3Hz
p - p	RMS
.03 γ	.006 γ

Fig. 6. Noise performance typical of the LFM sensors (see text).

response to a 0.1 γ p-p sinewave signal. Noise spectrum tests have shown that the noise amplitude decreases rapidly with increasing frequency (see Figure 7).

In addition to the use of multiple magnetometers and sensor 'flipping' to enhance the accuracy of the measurements, further calibration checks will be provided by occasional spacecraft roll maneuvers and by use of a minimum variance technique initially discussed by Davis and Smith (1968) and further developed by Belcher

(1973) and Hedgecock (1975). Based on a maximized error analysis, it is estimated conservatively that absolute accuracies of $\approx 0.09\ \gamma$ are achievable with the Voyager experiment. Of course, changes in the field which are much smaller than $0.09\ \gamma$ can

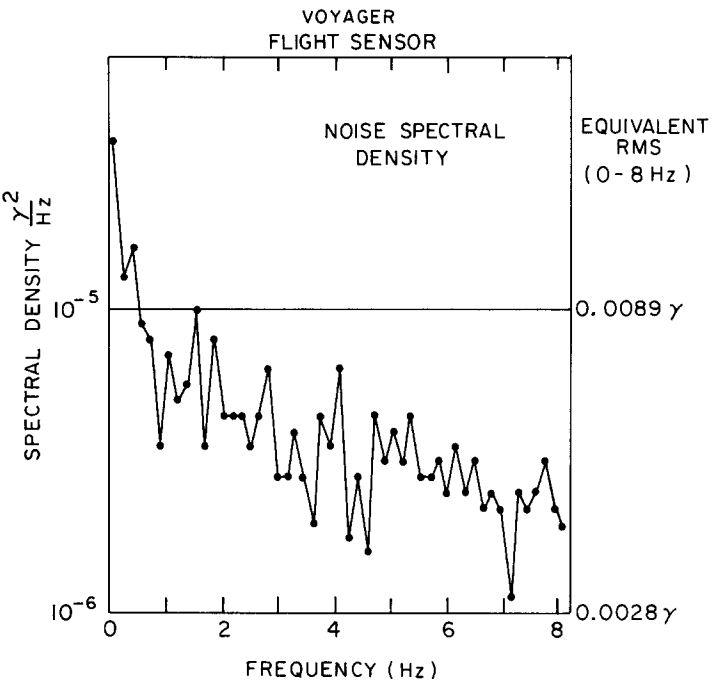

Fig. 7. Power spectrum of sensor noise data from tests performed in a cryogenic shield. The spectral shape is primarily due to the noise characteristics of the sensor and sensor electronics. The spectral density equivalent of an rms noise level of $0.006\ \gamma$ is $4.3\times10^{-6}\ \gamma^2\ \mathrm{Hz}^{-1}$. This can be compared with the quantization noise levels of $1.9\times10^{-7}\ \gamma^2\ \mathrm{Hz}^{-1}$ in the $\pm 8.8\ \gamma$ range and $1.6\times10^{-6}\ \gamma^2\ \mathrm{Hz}^{-1}$ in the $\pm 26\ \gamma$ range.

be detected, since their observation is limited only by the quantization step size ($0.004\ \gamma$ in the most sensitive range) and the RMS noise level of the sensors ($0.006\ \gamma$). This is important for studies of very low amplitude waves.

5.6. Data Modes and Onboard Processing

The data handling scheme is an important feature of this experiment, because the telemetry bandwidth available to the experiment will be reduced each time the spacecraft telemetry rate is reduced at distances from the Sun of typically 2.6, 3.3, 5.0, 7.0 and 9.0 AU. At encounters, the bandwidth available to science will be increased to permit intensive study of detailed phenomena at the planets. The schedule of successive reductions in telemetry bandwidth available to the experiment with increasing heliocentric distance during cruise requires an adaptive onboard data processing scheme that maintains a high rate of information transfer while providing the required reduction in the data transmission rate.

In order to accomplish these objectives, the experiment data system was designed to produce either direct readout, time averaging, 6-bit differencing or adaptive 2-bit delta modulation (DM) of the data. The onboard data processing that is done within the experiment hardware itself consists primarily of the storing, formating and shifting of data to the spacecraft Flight Data Subsystem (FDS), as well as command decoding and other housekeeping. All higher level data processing (averaging, differencing and DM) is performed for the experiment by the FDS.

The selection of data mode depends on available bandwidth, going to increasingly more dense data compaction up to reductions of approximately 6 to 1 as the bandwidth is reduced. The various modes and their associated data rates are shown in detail in Table II. In the table, P and S designate the LFM 'primary' and 'secondary' systems, respectively. System P could be associated with either the inner or the outer LFM sensor, but for the nominal experiment it designates the outboard sensor and S the inner.

The basic measurement sampling rate of the LFM's in all modes is $16\frac{2}{3}$ vector samples/sec. In the straight averaging mode only simple averaging of measurements is used for data compaction. In general, there are N_P and N_S points per average for systems P and S, respectively. This mode is the most conservative, as measured by $WPS_{TOTAL} = WPS_P + WPS_S$, where WPS is the rate of vector (3 component) words (measurement or averaged measured points) per second. In the 6-bit differencing mode, 6-bit differences of averages and less frequently full 12-bit reference averages are telemetered to ground. The ratios of the number of 6-bit to reference words for a given submode are given by K_P and K_S. The reference words are redundant under ideal conditions except for initialization purposes, but in general they will be used to correct for possible 6-bit saturation or other possible telemetry errors.

The adaptive 2-bit delta modulation mode is a very robust and 'efficient' data compaction scheme, yielding a broad band of information for the low bit rates available at the greatest heliocentric distances. The DM system used in the Voyager experiment is an improved version of systems flown successfully in the experiments on Explorers 47 and 50 and Mariner 10. All are 2-step predictor-corrector devices (Moyer, 1968). The DM mode is analogous to the 6-bit differencing mode, except that the 6-bit difference of averages is replaced with 2-bit delta modulation of averages. For each case in each mode in Table II, the WPS values indicate the effective information rate for that case, after reconstruction on the ground of the measurement averages.

In the cruise mode, only the LFM's will be operated, whereas both LFM and HFM systems will be in operation during planetary and satellite encounters. For the HFM's the basic sampling rate is $1\frac{2}{3}$ vectors/sec, the telemetry rate is 120 BPS equally divided between inboard and outboard measurements, and WPS = 1.67 for each.

Appropriate housekeeping parameters such as data mode, instrument range, critical temperatures and voltages are monitored periodically and read out into the telemetry stream at a low bit rate. Changes in the experiment's mode of operation are implemented in synchronization with such readouts.

6. Summary

The magnetic field experiment will provide precise and accurate measurements of magnetic fields in the outer solar system and possibly also in the interstellar medium during the Voyager missions. The wide dynamic ranges of the magnetometer systems (±0.5 G for the LFM's, ±20 G for the HFM's) will insure that the objectives of measuring the planetary fields of Jupiter, Saturn, and possibly Uranus are met. On the basis of past direct measurement at Jupiter and an inferred Saturnian field, maximum fields expected to be observed along the trajectories at Jupiter and Saturn are approximately 0.036 G (3600 γ) and 0.027 G (2700 γ), respectively. Both are well within the LFM total dynamic range. However, the forty-fold increase in HFM range over that of the LFM's allows for the fact that the fields at Saturn and Uranus have never been directly measured and could be much larger than expected. Also there is the possibility that nominal trajectories will not be flown.

TABLE II

Voyager magnetometer LFM data modes

Cruise modes	AU	MAG BPS	P BPS	N_P	S BPS	N_S	Full 12-bit words P BPS	N_P	S BPS	N_S	Vector WPS P WPS	S WPS
Straight averaging mode	1.0	1200					600	1	600	1	16.667	16.667
	2.6	450					300	2	150	4	8.333	4.167
	3.3	187.5					150	4	37.5	16	4.167	1.042
	5.0											
			6-Bit differencing words									
6-Bit differencing mode	5.0	93.75	75	4	7.5	40	7.5	K_P 20	3.75	K_S 4	4.167	0.417
	7.0											
			2-Bit DM words									
Delta modulation mode	7.0	46.875	25	4	12.50	8	4.688	32	4.688	16	4.166	2.083
	9.0	5.938	3.125	32	1.563	64	0.625	30	0.625	15	0.521	0.260
			6-Bit differencing words									
Encounter mode		630	300	1	150	2	120	5	60	5	16.667	8.333

Basic Sampling Rate is $16\frac{2}{3}$ vectors/sec in all Modes.
Symbols: P = Primary mag. S = Secondary mag. N = Samples/Average. See text for other definitions.

Other major objectives of this mission are: to study the interactions of the solar wind with planetary fields; to investigate the interactions of satellites with planetary fields and perhaps with the solar wind in some cases; to search for evidence of internal satellite fields when near-encounters with satellites are achieved; and to study the large-scale structure of the interplanetary magnetic field and the physics of

interplanetary microscale phenomena. To achieve these objectives, particularly those in which the physics of such processes as merging, reconnection, plasma instabilities, plasma sheets, and current systems are to be studied in detail, the LFM design permits absolute accuracies to $<0.1\ \gamma$ to be attained and field changes $>0.006\ \gamma$ to be directly observed.

The experiment data system has been designed to continue providing a relatively high effective information rate even as the telemetry bandwidth is reduced at large distances from the sun through use of increasingly efficient data compaction modes. The effective rate varies from the full basic LFM sampling rate of $16\frac{2}{3}$ vectors/sec near 1 AU and at encounters (primary LFM, reconstructed from 6-bit differences) to a minimum of 0.5 vectors/sec (primary LFM, reconstructed from 2-bit DM words) at heliocentric distances of 10 AU and greater.

To insure long term reliability on a mission lasting ≥ 4 years, the instrument design includes both dual magnetometer systems and redundancy of all critical internal functions. In addition, the dual LFM configuration permits removal of the magnetic field of the space-craft (expected to be $\leq 0.2\ \gamma$ at the outboard LFM) from the measurements throughout the mission.

In addition to their fundamentally important direct contributions, the magnetic field measurements will complement the Voyager plasma and energetic particle measurements and radio astronomy observations, both in the vicinity of the planets and in interplanetary space.

Acknowledgements

We wish to thank our colleagues at Goddard Space Flight Center, D. R. Howell, C. S. Scearce, J. L. Scheifele, J. B. Seek, W. C. Stange and E. M. Worley, and especially G. A. Sisk at JPL, for their many important technical contributions to the development of this experiment. We also wish to acknowledge the contributions of J. R. Hodge and F. H. Hunsaker at GSFC, and the members of the Voyager Project staff and supporting technical groups at JPL.

References

Acuna, M. H.: 1974, *IEEE Trans. Magnetics, MAG*-10, 519,
Acuna, M. H. and Ness, N. F.: 1976a, in T. Gehrels (ed.), *Jupiter*, Univ. of Arizona Press, Tucson, p. 830.
Acuna, M. H. and Ness, N. F.: 1976b, *J. Geophys. Res.* **81**, 2917.
Axford, W. I.: 1973, *Space Sci. Rev.* **14**, 582.
Barish, F. D. and Smith, R. A.: 1975, *Geophys. Res. Lett.* **2**, 269.
Belcher, J. W.: 1973, *J. Geophys. Res.* **78**, 6480.
Bok, B. J.: 1970, in W. Becker and G. Contopoulos (eds.), 'The Spiral Structure of our Galaxy', *IAU Symp.* **38**, 457.
Brown, L. W.: 1975, *Astrophys. J.* **198**, L89.
Brown, L. W.: 1976, *Astrophys. J.* **207**, L209.
Burlaga, L. F.: 1975, *Space Sci. Rev.* **17**, 327.
Fairfield, D. H.: 1976, in D. J. Williams (ed.), *Physics of Solar Planetary Environments, Vol. II*, AGU, p. 511.

Fairfield, D. H. and Behannon, K. W.: 1976, *J. Geophys. Res.* **81**, 3897.
Frank, L. A., Ackerson, K. L., Wolfe, J. H., and Mihalov, J. D.: 1976, *J. Geophys. Res.* **81**, 457.
Gleeson, L. F. and Axford, W. I.: 1976, *J. Geophys. Res.* **81**, 3403.
Goertz, C. K.: 1976, *J. Geophys. Res.* **81**, 3368.
Goldreich, P. and Lynden-Bell, D.: 1969, *Astrophys. J.* **156**, 59.
Gosling, J. T., Hundhausen, A. J., and Bame, S. J.: 1976, *J. Geophys. Res.* **81**, 2111.
Greenstadt, E. W.: 1976, in B. M. McCormac (ed.), *Magnetospheric Particles and Fields*, D. Reidel, Dordrecht, Holland, p. 13.
Gurnett, D. A.: 1972, *Astrophys. J.*, **175**, 525.
Hedgecock, P. C.: 1975, *Space Sci. Instrumentation*, **1**, 83.
Hundhausen, A. J.: 1972, *Coronal Expansion and Solar Wind*, Springer-Verlag, New York.
Hundhausen, A. J. and Gosling, J. T.: 1976, *J. Geophys. Res.* **81**, 1436.
Ipavich, F. M. and Lepping, R. P.: 1975, in Conference Papers of the 14th International Cosmic Ray Conference, Munich, FRG, Vol. 5, p. 1829.
Mead, G. D.: 1974, *J. Geophys. Res.* **79**, 3514.
Moyer, C. V.: 1968, NASA-GSFC X-616-68-453.
Ness, N. F., Behannon, K. W., Lepping, R. P., and Schatten, K. H.: 1971, *J. Geophys. Res.* **76**, 3564.
Neubauer, F. M.: 1975, *J. Geophys. Res.* **80**, 3235.
Neubauer, F. M. and Luzemann, M.: 1977, in preparation.
Shawhan, S. D.: 1976, *J. Geophys. Res.* **81**, 3373.
Siscoe, G. L.: 1975, *Icarus* **24**, 311.
Smith, E. J., Davis, L. Jr., Jones, D. E., Coleman, P. J. Jr., Colburn, D. S., Dyal P., Sonett, C. P. and Frandsen, A. M. A.: 1974, *J. Geophys. Res.* **79**, 3501.
Smith, E. J., Davis, L. Jr., Jones, D. E., Coleman, P. J. Jr., Colburn, D. S., Dyal, P. and Sonnett, C. P.: 1975, *Science* **188**, 451.
Smith, E. J., Davis, L. Jr., and Jones, D. E.: 1976a, in T. Gehrels (ed.), *Jupiter*, Univ. of Arizona Press, Tucson, p. 788.
Smith, E. J., Davis, L. Jr., Coleman, P. J. Jr., Coleburn, D. S., Dyal, P. and Jones, D. E.: 1967b, *J. Geophys. Res.* (in press).
Smith, E. J. and Wolfe, J. H.: 1976, *Geophys. Res. Lett.* **3**, 137.
Smith, R. A.: 1976, in T. Gehrels (ed.), *Jupiter*, Univ. of Arizona Press, Tucson, p. 1146.
Thompson, R. F. and Ness, N. F.: 1977, *J. Geophys. Res.* (submitted).
Tainor, J. H., McDonald, F. B., Teegarden, B. J., Webber, W. R., and Roelof, E. C.: 1974, *J. Geophys. Res.* **79**, 3600.
Vershuur, G. L.: 1968, *Phys. Rev. Lett.* **21**, 775.
Webster, D. L., Alksne, A. Y. and Whitten, R. C.: 1972, *Astrophys. J.* **174**, 685.
Wolfe, J. H., Mihalov, J. D., Collard, H. R., McKibben, D. D., Frank, L. A., and Intriligator, D. S.: 1974, *J. Geophys. Res.* **79**, 3489.
Yung, Y. L. and McElroy, M. B.: 1975, *Bull. AAS* **7**, 387.